Journal of Materials Chemistry B

Silica-Coated Gold Nanorods with Hydrophobic Modification Show Both Enhanced Two-Photon Fluorescence and Ultrasound Drug Release

Journal:	*Journal of Materials Chemistry B*
Manuscript ID	TB-COM-10-2022-002197.R1
Article Type:	Communication
Date Submitted by the Author:	10-Nov-2022
Complete List of Authors:	Mueller, Evan; University of Colorado Boulder, Chemical and Biological Engineering Alina, Talaial; University of Colorado Boulder, Chemical and Biological Engineering Curry, Shane; University of Colorado Boulder, Chemical and Biological Engineering Ganguly, Saheli; University of Colorado, Chemistry and Biochemistry Cha, Jennifer; UCSD, Nanoengineering Goodwin, Andrew; University of Colorado Boulder, Chemical and Biological Engineering

COMMUNICATION

Silica-Coated Gold Nanorods with Hydrophobic Modification Show Both Enhanced Two-Photon Fluorescence and Ultrasound Drug Release

Received 00th January 20xx,
Accepted 00th January 20xx

DOI: 10.1039/x0xx00000x

Evan N. Mueller,[a,†] Talaial B. Alina, [a,†] Shane D. Curry,[a] Saheli Ganguly,[a] Jennifer N. Cha,[a,*] and Andrew P. Goodwin[a,*]

Hydrophobically-modified silica-coated gold nanorods are presented here as multifunctional theranostic agents. The single modification both increases two-photon fluorescence and promotes cavitation-based acoustic signal for imaging. A two-fold greater release of small molecule drugs was observed under ultrasound-mediated conditions as compared to passive release without ultrasound.

Many anticancer chemotherapies lack the ability to specifically target cancer cells. Such drugs require significant systemic dosing, which in turn can cause many negative side effects such as hair loss, nausea, fatigue, and others.[1] Determining the efficacy of treatment is also not always straightforward. For example, it is difficult to distinguish between a poor response caused by resistance to the therapeutic and one caused by poor delivery.

Theranostics, or agents that are capable of both diagnosis and therapy, directly address this latter concern. These materials often possess a passively releasing or externally inducible therapeutic component along with contrast agents for real-time imaging.[2,3] Thus, they can be tracked to view their distribution in the patient or even see real-time information about the efficacy of treatment. Nanoparticles in particular offer a unique canvas for imparting multiple functions in one carrier, including detection by light, ultrasound, magnetic fields (MRI), x-ray, and PET.[4–7] To keep nanoparticles dispersed in aqueous and biologically relevant media, they must be functionalized with ligands to prevent or reduce aggregation as well as impart biocompatibility. But functionalization can also enhance existing properties in the nanostructures, or even impart new properties altogether.

[a] *Department of Chemical and Biological Engineering, University of Colorado, 596 UCB, Boulder, Colorado 80309, United States.*
† These authors contributed equally to this manuscript.
Electronic Supplementary Information (ESI) available: [details of any supplementary information available should be included here]. See DOI: 10.1039/x0xx00000x

Ultrasound has several useful properties for directing localized treatment.[8,9] First, ultrasound can penetrate most soft tissues and can be focused down to millimeter resolution even in the abdomen.[10] These lower intensity waves can disrupt structures such as liposomes to release drugs, though the release yield can be low.[11–13] Release rates can be increased by raising the ultrasound intensity to levels capable of inducing cavitation.[13] However, high intensity focused ultrasound (HIFU) must be focused using image guidance to detect the location of accumulated nanoparticles to reduce the risk of off-target tissue side effects.

Previous research in our labs has examined how functionalization can reduce the amount of energy required to induce cavitation in a specific volume.[6,14,15] Cavitation processes tend to proceed by heterogeneous nucleation, in which the bubble forms on a solid-liquid interface rather than in the liquid alone, due to favorable energy of bubble formation at the interface.[16,17] To take advantage of the thermodynamics of bubble nucleation, in previous work we functionalized silica nanoparticles with hydrophobic alkyl chains, then suspended the nanoparticles with amphiphiles.[6,15] Thus, cavitation can occur at lower input ultrasound energies, thus confining cavitation (and tissue damage) to areas with localized nanoparticles.[15] This research was extended to photoacoustic contrast agents containing gold nanorods (AuNRs) capable of absorbing light in the near infrared (NIR) range.[18] These AuNRs were coated with mesoporous silica, then functionalized with hydrophobic alkyl groups. Cavitation response from these nanoparticles increased the photoacoustic response that could be generated by the silica nanoparticles by 12x compared to the silica coated gold nanorods at a laser fluence of only 20 mJ/cm^2.[18]

Multiphoton microscopy is a powerful tool for diagnosis and imaging. Multiphoton microscopy offers better image resolution than confocal microscopy and has been developed for deep tissue imaging, particularly for brain imaging.[19,20] In vivo imaging requires NIR light excitation, which has lower

scattering and absorption properties in tissue compared to visible and UV light.[21] In addition to a high TPA cross section of >2300 GM,[22,23] gold nanorods boast higher biocompatibility than other nanoparticles with high TPAs such as upconversion nanoparticles.[24–27] Although gold nanorods can melt under extended NIR irradiation, the introduction of a silica layer can slow this process for enhanced optical and photoacoustic imaging.[28,29]

In this work, we show that phospholipid-stabilized, hydrophobically-modified mesoporous silica-coated gold nanorods (PL-HMSiO2-AuNRs) are capable of not only enhanced multiphoton imaging but also acoustically-triggered drug release. First, we show that nanorod fluorescence decays more slowly under femtosecond fluorescence microscopy, thus allowing greater imaging acquisition per nanorod. While functionalized and unfunctionalized silica show similar imaging profiles at low laser incidences, at higher laser powers the signal decay time increases for PL-HMSiO2-AuNRs. Second, these functionalized AuNRs could encapsulate and release hydrophobic drugs such as paclitaxel (PTX), which requires amphiphiles for formulation in aqueous media as its bioavailability is insufficient on its own. Release profiles of the PTX loaded particles showed ~two-fold greater drug release upon HIFU insonation, with significantly improved cell cytotoxicity as compared to PTX-surfactant complexes. Taken together, these results show how a single hydrophobic modification of silica-coated gold nanorods enhanced both imaging and drug release in the same theranostic nanostructure.

Results and Discussion

Gold nanorods (AuNRs) were first synthesized using published procedures[30] followed by a coating of mesoporous silica.[18,31] Briefly, gold nanorods were prepared from gold (III) trihydride using sodium oleate and cetrimonium bromide (CTAB) as stabilizing agents to yield AuNRs with a length of 137.5 ± 14.7 nm and a width of 52.0 ± 2.5 nm and a plasmon resonance at 757 nm with a FWHM of 159 nm.[30] The as-synthesized AuNRs were reacted with tetraethylorthosilicate (TEOS) at pH ~11 in the presence of 1.7 mM CTAB to produce mesoporous silica coated AuNRs (MSiO2-AuNR). The silica coating on the AuNRs was measured by TEM to be ~16.5 nm (Figure 1). Next, the remaining CTAB was removed by reacting the silica coated gold nanorods with acidified methanol at 65 °C for 1 h, and then washing with methanol to remove the excess CTAB. The MSiO2-AuNRs were then reacted with hydrophobic dodecyltrichlorosilane (DDTS) to create the hydrophobically-modified MSiO2-AuNRs (HMSiO2-AuNRs). Finally, the hydrophobically-modified particles were resuspended in a mixture of 1,2-dipalmitoyl-sn-glycero-3-phosphocholine (DPPC) and 1,2-distearoyl-sn-glycero-3-phosphoethanolamine-N-[methoxy(polyethylene glycol)-2000] (DSPE-PEG2000-methoxy) to stabilize the nanoparticles (PL-HMSiO2-AuNRs) in water. The final particle suspension had a longitudinal surface plasmon resonance (LSPR) peak at 790 nm, which was red shifted from the LSPR of the as-synthesized AuNR at 758 nm.

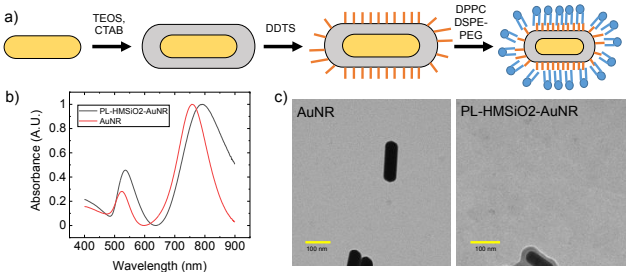

Figure 1. a) General synthesis scheme of PL-HMSiO2-AuNRs. B) Normalized UV-Vis spectra of the AuNRs and PL-HMSiO2-AuNRs. C) TEM images of the AuNRs and PL-HMSiO2-AuNRs.

Next, the MSiO2-AuNR and PL-HMSiO2-AuNRs were tested for multiphoton fluorescence at their LSPRs, tracking by multiphoton microscopy (70 fs, 80 MHz) at different input laser powers in two-minute movie segments. At laser powers below about 300 mW, both MSiO2-AuNR and PL-HMSiO2-AuNR rods produced the same light intensity over the entire recorded movie (Figure S2). Above 300 mW, a divergence was seen between the unmodified (MSiO2-AuNRs) and hydrophobically modified (PL-HMSiO2-AuNRs) nanorods (Figure 2). This difference in intensity increased with increasing laser power, with the PL-HMSiO2-AuNRs showing 48% greater intensity at ten seconds irradiation at 400 mW. The MSiO2-AuNRs showed a strong fluorescence initially, but the signal decayed quickly. After fitting the recorded signal losses to exponential decay functions, the hydrophobic modification of the nanorods was found to increase the signal half-life from 1.35 ± 0.13 s to 5.61 ± 0.69 s for unfunctionalized silica-coated AuNRs (MSiO2-AuNR) as compared to functionalized nanorods (PL-HMSiO2-AuNRs). At 120 s of acquisition time, the integrated signal of the PL-HMSiO2-AuNRs was within error of the unfunctionalized MSiO2-AuNR (Figure S3). Because emission was measured by imaging rather than fluorimetry, the measured results are independent of nanorod concentration, and thus differences in emission can be ascribed to individual nanorod structures. Thus, the PL-HMSiO2-AuNRs showed a greater stability to fs pulsed multiphoton imaging than MSiO2-AuNRs did and could be used to acquire brighter images. We posit two reasons for this increase in stability. First, the hydrophobic coating may resist gold expansion due to the unfavorable interactions between gold and the alkyl chains as compared to the unfunctionalized rods, providing a longer window of irradiation. Second, the added alkyl chains and PEG-lipids may thermally insulate the gold nanorods from the surrounding medium. It has, for example, been shown that gold nanorods with increasing mass of PEG coating allows gold nanorods to maintain their shapes upon exposure to laser incident light.[32]

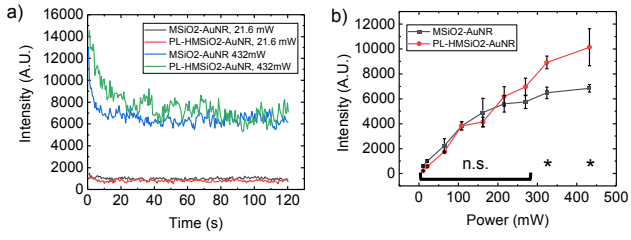

Figure 2. a) Time-resolved two-photon luminescence at 21.8 mW and 432 mW of input laser power. b) Intensity of two-photon luminescence of PL-HMSiO2-AuNR and the MSiO2-AuNR at 10 s irradiation at different input laser powers. *, $p < 0.5$; n.s,. $p > 0.05$.

Next, the MSiO2-AuNRs and PL-HMSiO2-AuNRs were tested for their ability to release drugs upon administration of HIFU. As discussed above, because a hydrophobic coating on silica nanostructures had previously shown an ability to enhance cavitation response under HIFU, the cavitation threshold of each nanorod sample was measured. In this setup (Figure S4), HIFU peak pressure was increased until signals above the noise floor could be measured on a passive cavitation detection transducer (20 MHz, Olympus). For PL-HMSiO2-AuNRs, the cavitation threshold was found to reside at a peak negative pressure of 10.61 MPa (Figure 3, S5). In contrast, for both MSiO2-AuNRs and a water blank, no significant cavitation was found up to a peak negative pressure (PNP) of 13.94 MPa, the highest pressure tested in this system. These findings were supported by images acquired on a Sequoia Acuson 512 ultrasound scanner (Figure 3). Briefly, images recorded in cadence pulse sequencing mode (specifically sensitive to bubbles[33]) showed the absence of signal at a PNP of 7.19 MPa for the PL-HMSiO2-AuNRs and the presence of signal at a PNP of 11.67 MPa for the PL-HMSiO2-AuNRs, consistent with the formation of cavitation bubbles. The dual confirmation of bubble formation by two detection techniques, as well as the presence of a specific cavitation threshold,[34] provided confidence that at 11.67 MPa acoustic cavitation was occurring on the PL-HMSiO2-AuNRs only.

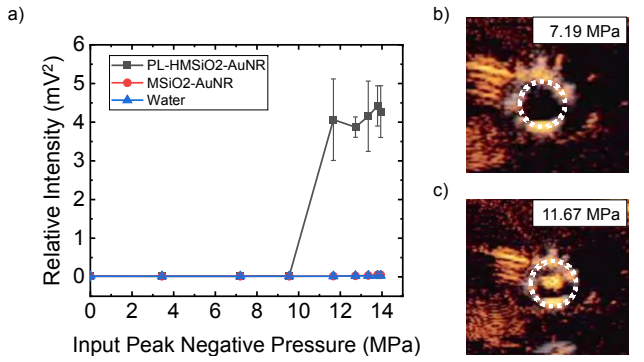

Figure 3. a) Intensity of received acoustic signal vs. input HIFU pressure from the PL-HMSiO2-AuNR, MSiO2-AuNR, and water. b, c) Cavitation response of the particles at a PNP of b) 7.19 MPa and c) 11.6 MPa. The white dotted circles indicate the location of the sample holder.

These results prompted an investigation into whether cavitation could increase the rate of drug release from the porous silica coating on the AuNRs. As a proof-of-concept study, DiO, a membrane dye likely to intercalate with the phospholipid monolayer surrounding the nanoparticles, was encapsulated in the nanorods[35] by mixing the dye with phospholipids in chloroform during the phospholipid capping step (see above). The DiO encapsulation efficiency (mass of DiO per mass DiO fed) was calculated to be 38.5 ± 7.9%, whereas dye loading (mass of DiO per mass particle) was calculated to be 5.1 ± 1.0% These were calculated by normalizing the nanoparticles' UV-Vis spectra to their LSPRs, then subtracting the UV-Vis spectra of the unloaded from the loaded nanoparticles to find the DiO concentration (Figure S6). Without hydrophobic modification of the silica-coated gold nanorods, DiO could not be loaded. Next, HIFU was applied to induce DiO release. HIFU was first applied for 2.5, 5, or 10 min at a PNP of 13.94 MPa, which is above the cavitation threshold of the PL-HMSiO2-AuNRs (Figure 3). A decrease in DiO fluorescence was observed with increasing HIFU insonation time (Figure S7). In standardizing these results to the initial amounts of encapsulated DiO, administration of HIFU resulted in the release of 22.1, 38.1, 42.2, and 48.1% of loaded DiO for the 0 (no HIFU, passive release), 2.5, 5 and 10 min of HIFU irradiation, respectively.

Based on the DiO studies, we next investigated PL-HMSiO2-AuNRs for loading the anticancer agent paclitaxel (PTX) and its release upon HIFU. Approximately 100 µg PTX were loaded per mg of PL-HMSiO2-AuNR by mixing the AuNRs with PTX in chloroform and evaporating the solvent. The encapsulation efficiency was determined to be 71.9 ± 7.7% and the drug loading was 10.6 ± 1.1% for PTX in the PL-HMSiO2-AuNRs. Samples in plastic pipettes were placed in a water bath with an aligned HIFU transducer and either insonated with HIFU with a peak negative pressure (PNP) of 13.94 MPa (active release) or not subjected to HIFU (passive release). Silica nanoparticles are known to show passive drug release with half-lives on the order of a few hours, which is consistent with the results reported here (Figure S8).[36] However, the application of HIFU led to a two-fold increase in burst release of PTX (Figure 4). This release mode was followed by a slow but steady zero-order release from the nanoparticles that was only observed with HIFU insonation (Figure 4). Because more than one kinetic mode appears to be present, we hypothesize that the structure of the PL-HMSiO2-AuNR allows drug to be loaded in two parts: in the pores of the silica and at the surface of the particle sandwiched by the phospholipid monolayer. As a result, each of these mechanisms of binding has its own adhesion energy and thus its own release profile. When HIFU is applied, the PTX is shed from the lipid layer, causing burst release. The missing lipids then allow PTX to exit internal pores in the silica structure. This kinetic mode is supported most directly by literature reports of zero-order release from silica structures following sonication.[37] In addition, similar zero-order profiles have been reported from silica[38] and other[39,40] nanoparticle structures.

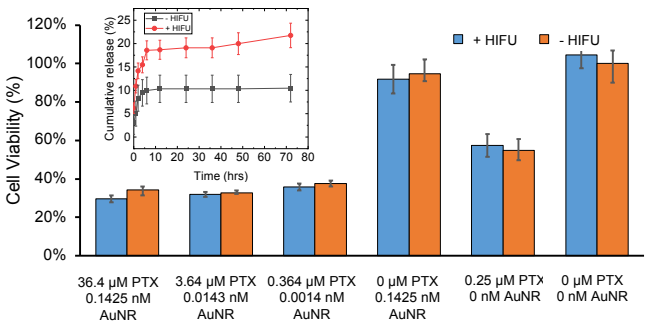

Figure 4. (a) MTT viability assay of MDA-MB-468 breast cancer cells against PTX-loaded

PL-HMSiO2-AuNRs, with (left, blue) and without (right, orange) HIFU. Concentrations of both PTX and AuNRs given in x-axis. Error bars indicate SEM. Inset: Release of PTX from PL-HMSiO2-AuNR with and without HIFU.

Next, the effects of both HIFU exposure and PTX loading on cell toxicity were tested with PL-HMSiO2-AuNRs. MDA-MB-468 human breast cancer cells were grown in standard 96-well plates to near confluence. Next, PL-HMSiO2-AuNRs with and without PTX loading were incubated with the cells for 1 h to allow particle binding and uptake. These particles were subjected to 2.5 min HIFU at 1.1 MHz, 10 Hz repetition rate, and 13.94 MPa to induce PTX drug release. Cell viability was then measured by MTT assay 24 h later (Figure 4). Without PTX, the administration of HIFU did not significantly increase cell death. This observation is consistent with previous studies that showed that cell death could be minimized if the HIFU pulse repetition rate was maintained at a low enough level (e.g. 10 Hz).[8] With PTX loaded into the AuNRs, significant (>60%) cell toxicity was observed for PTX equivalent concentrations of 36.4, 3.64, and 0.364 μM. Interestingly, for 0.25 μM PTX without AuNRs, only 57.5% cell viability was observed, thus showing less toxicity than a similar amount of PTX with AuNRs. While HIFU causes PTX release from the AuNRs, it is likely that the PTX from passive release was still sufficient to induce significant cell toxicity. Without gold nanorods, the effect of HIFU on PTX toxicity was not significant. To support these findings, confocal microscopy images of DiO-loaded PL-HMSiO2-AuNRs incubated with MDA-MB-468 cells showed that DiO fluorescence was inside the cells after 5 h (Figure S9).

In this study, hydrophobic modification of silica-coated gold nanorods provided increased performance in both imaging and therapy. First, the modification resulted in a 48% greater two-photon fluorescence imaging lifetime than nanorods without hydrophobic functionalization. The addition of these hydrophobic groups also allowed detection of cavitation events under HIFU insonation. The ability to load hydrophobic drugs and fluorophores was demonstrated, as was HIFU-mediated release. Finally, the PL-HMSiO2-AuNRs loaded with PTX showed significant (>60%) cell killing against human breast cancer cells. Future avenues for study are the effect of gold nanorod size on two-photon fluoresecence,[41–43] and modifying release rates to have better control of the onset of zero-order release. Taken together, this work shows how functionalization can increase the performance of both imaging and therapy in nanoscale theranostics.

Acknowledgements

The authors acknowledge NSF CBET 2025547 for support of this research. We also acknowledge the Light Microscopy Core Facility at the University of Colorado Boulder (RRID:SCR_018993) and Dr. James D. Orth for help and advice with multiphoton microscopy. Finally, we thank Prof. Ted Randolph for use of his DLS instrument and Prof. Todd Murray for use of his HIFU transducer.

Conflicts of interest

There are no conflicts to declare.

Notes and references

1 M. Goodman, Seminars in Oncology Nursing, 1989, 5, 29–52.
2 E.-K. Lim, T. Kim, S. Paik, S. Haam, Y.-M. Huh and K. Lee, Chem. Rev., 2015, 115, 327–394.
3 S. S. Kelkar and T. M. Reineke, Bioconjugate Chem., 2011, 22, 1879–1903.
4 L. He, C. Mao, M. Brasino, A. Harguindey, W. Park, A. P. Goodwin and J. N. Cha, ACS Appl. Mater. Interfaces, 2018, 10, 27965–27971.
5 L. He, J. Dragavon, S. Cho, C. Mao, A. Yildirim, K. Ma, R. Chattaraj, A. P. Goodwin, W. Park and J. N. Cha, J. Mater. Chem. B, 2016, 4, 4455–4461.
6 A. Yildirim, R. Chattaraj, N. T. Blum, G. M. Goldscheitter and A. P. Goodwin, Adv. Healthcare Mater., 2016, 5, 1290–1298.
7 J. M. Bryson, K. M. Fichter, W.-J. Chu, J.-H. Lee, J. Li, L. A. Madsen, P. M. McLendon and T. M. Reineke, Proc. Natl. Acad. Sci. U.S.A., 2009, 106, 16913–16918.
8 A. Yildirim, R. Chattaraj, N. T. Blum, D. Shi, K. Kumar and A. P. Goodwin, Adv Healthcare Materials, 2017, 6, 1700514.
9 A. Yildirim, D. Shi, S. Roy, N. T. Blum, R. Chattaraj, J. N. Cha and A. P. Goodwin, ACS Appl Mater Interfaces, 2018, 10, 36786–36795.
10 C. A. Speed, Rheumatology, 2001, 40, 1331–1336.
11 M. Mathiyazhakan, Y. Yang, Y. Liu, C. Zhu, Q. Liu, C.-D. Ohl, K. C. Tam, Y. Gao and C. Xu, Colloids and Surfaces B: Biointerfaces, 2015, 126, 569–574.
12 Ž. Pandur, I. Dogsa, M. Dular and D. Stopar, Ultrasonics Sonochemistry, 2020, 61, 104826.
13 Y.-S. Kim, M. J. Ko, H. Moon, W. Sim, A. S. Cho, G. Gil and H. R. Kim, Pharmaceutics, 2022, 14, 1314.
14 A. Yildirim, R. Chattaraj, N. T. Blum and A. P. Goodwin, Chem. Mater., 2016, 28, 5962–5972.
15 N. T. Blum, A. Yildirim, C. Gyorkos, D. Shi, A. Cai, R. Chattaraj and A. P. Goodwin, ACS Appl. Mater. Interfaces, 2019, 11, 15233–15240.
16 D. Ben-Amotz, The Journal of Chemical Physics, 2005, 123, 184504.
17 K. A. Mørch, J Hydrodyn, 2009, 21, 176–189.
18 E. N. Mueller, M. Kuriakose, S. Ganguly, K. Ma, M. A. Inzunza-Ibarra, T. W. Murray, J. N. Cha and A. P. Goodwin, ACS Appl. Nano Mater., 2021, 4, 12073–12082.
19 L. Streich, J. C. Boffi, L. Wang, K. Alhalaseh, M. Barbieri, R. Rehm, S. Deivasigamani, C. T. Gross, A. Agarwal and R. Prevedel, Nat Methods, 2021, 18, 1253–1258.
20 D. R. Miller, J. W. Jarrett, A. M. Hassan and A. K. Dunn, Current Opinion in Biomedical Engineering, 2017, 4, 32–39.
21 W. Denk, J. H. Strickler and W. W. Webb, Science, 1990, 248, 73–76.
22 H. Wang, T. B. Huff, D. A. Zweifel, W. He, P. S. Low, A. Wei and J.-X. Cheng, Proc. Natl. Acad. Sci. U.S.A., 2005, 102, 15752–15756.
23 N. Gao, Y. Chen, L. Li, Z. Guan, T. Zhao, N. Zhou, P. Yuan, S. Q. Yao and Q.-H. Xu, J. Phys. Chem. C, 2014, 118, 13904–13911.
24 J. Olesiak-Banska, M. Waszkielewicz, P. Obstarczyk and M. Samoc, Chem. Soc. Rev., 2019, 48, 4087–4117.
25 D.-S. Wang, F.-Y. Hsu and C.-W. Lin, Opt. Express, 2009, 17, 11350.
26 T. Wang, D. Halaney, D. Ho, M. D. Feldman and T. E. Milner, Biomed. Opt. Express, 2013, 4, 584.
27 N. J. Durr, T. Larson, D. K. Smith, B. A. Korgel, K. Sokolov and A. Ben-Yakar, Nano Lett., 2007, 7, 941–945.

28 Y.-S. Chen, W. Frey, S. Kim, P. Kruizinga, K. Homan and S. Emelianov, Nano Lett., 2011, 11, 348–354.
29 Y.-S. Chen, W. Frey, S. Kim, K. Homan, P. Kruizinga, K. Sokolov and S. Emelianov, Opt. Express, 2010, 18, 8867.
30 X. Ye, C. Zheng, J. Chen, Y. Gao and C. B. Murray, Nano Lett., 2013, 13, 765–771.
31 I. Gorelikov and N. Matsuura, Nano Lett., 2008, 8, 369–373.
32 R. Marasini, A. Pitchaimani, T. D. T. Nguyen, J. Comer and S. Aryal, Nanoscale, 2018, 10, 13684–13693.
33 S. M. Stieger, P. A. Dayton, M. A. Borden, C. F. Caskey, S. M. Griffey, E. R. Wisner and K. W. Ferrara, Contrast Media Molecular Imaging, 2008, 3, 9–18.
34 J. Haller and V. Wilkens, Ultrasound in Medicine & Biology, 2018, 44, 397–415.
35 Q. Lubart, J. K. Hannestad, H. Pace, D. Fjällborg, F. Westerlund, E. K. Esbjörner and M. Bally, Phys. Chem. Chem. Phys., 2020, 22, 8781–8790.
36 Q. He and J. Shi, J. Mater. Chem., 2011, 21, 5845.
37 M. S. Birajdar and J. Lee, Chemical Engineering Journal, 2016, 288, 1–8.
38 S. Bhattacharyya, H. Wang and P. Ducheyne, Acta Biomaterialia, 2012, 8, 3429–3435.
39 S. Fredenberg, M. Wahlgren, M. Reslow and A. Axelsson, International Journal of Pharmaceutics, 2011, 415, 34–52.
40 T. Kubota, Y. Kurashina, J. Zhao, K. Ando and H. Onoe, Materials & Design, 2021, 203, 109580.
41 W. Yim, R. M. Borum, J. Zhou, Y. Mantri, Z. Wu, J. Zhou, Z. Jin, M. Creyer and J. V. Jokerst, Nanotheranostics, 2022, 6, 79–90.
42 E. D. SoRelle, O. Liba, Z. Hussain, M. Gambhir and A. de la Zerda, Langmuir, 2015, 31, 12339–12347.
43 H.-D. Deng, G.-C. Li, Q.-F. Dai, M. Ouyang, S. Lan, V. A. Trofimov and T. M. Lysak, Nanotechnology, 2013, 24, 075201.